

Representing Long Volumetric Video with Temporal Gaussian Hierarchy

ZHEN XU*, State Key Lab of CAD&CG, Zhejiang University, China

YINGHAO XU*, Stanford University, United States

ZHIYUAN YU*, Hong Kong University of Science and Technology, China

SIDA PENG, Zhejiang University, China

JIAMING SUN, Zhejiang University, China

HUJUN BAO, State Key Lab of CAD&CG, Zhejiang University, China

XIAOWEI ZHOU[†], State Key Lab of CAD&CG, Zhejiang University, China

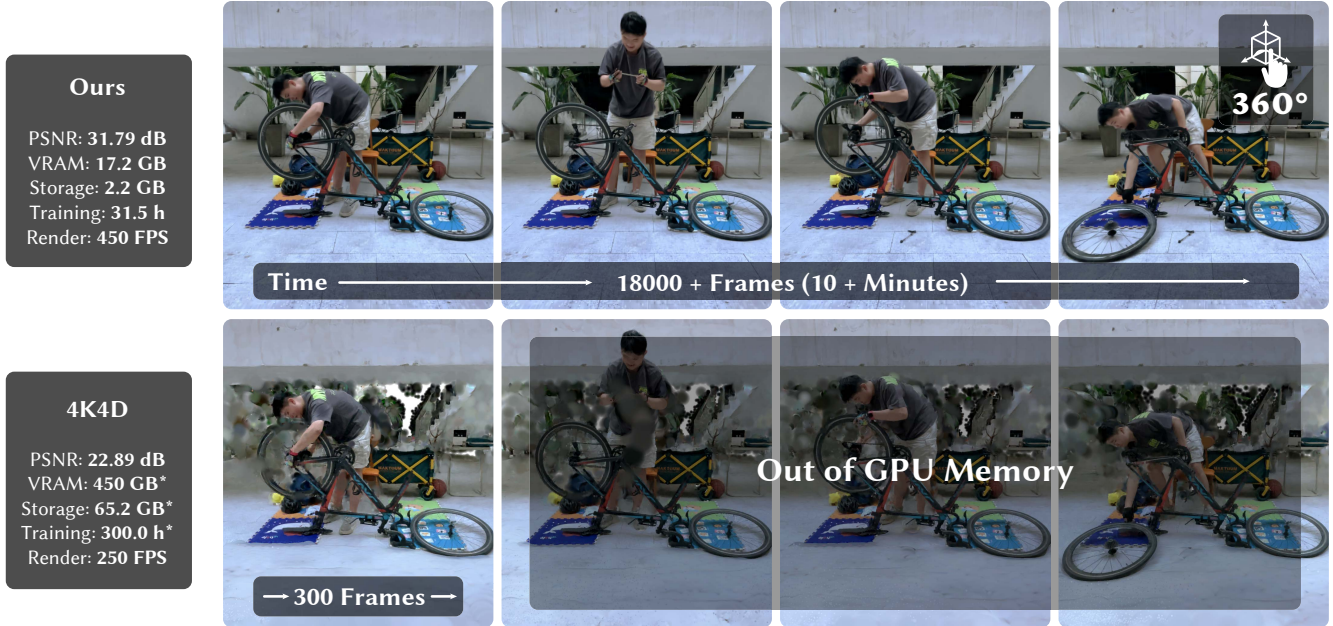


Fig. 1. **Photorealistic rendering of a long volumetric video with 18,000 frames.** Our proposed method utilizes an efficient 4D representation with Temporal Gaussian Hierarchy, requiring only 17.2 GB of VRAM and 2.2 GB of storage for 18,000 frames. This achieves a 30x and 26x reduction compared to the previous state-of-the-art 4K4D method [Xu et al. 2024b]. Notably, 4K4D [Xu et al. 2024b] could only handle 300 frames with a 24GB RTX 4090 GPU, whereas our method can process the entire 18,000 frames, thanks to the constant computational cost enabled by our Temporal Gaussian Hierarchy. Our method supports real-time rendering at 1080p resolution with a speed of 450 FPS using an RTX 4090 GPU while maintaining state-of-the-art quality.

This paper aims to address the challenge of reconstructing long volumetric videos from multi-view RGB videos. Recent dynamic view synthesis

*Denotes equal contribution.

[†]Corresponding author: Xiaowei Zhou.

Authors' addresses: Zhen Xu, zhenx@zju.edu.cn, State Key Lab of CAD&CG, Zhejiang University, Hangzhou, China; Yinghao Xu, justimyhxu@gmail.com, Stanford University, Stanford, United States; Zhiyuan Yu, zyuaq@ust.hk, Hong Kong University of Science and Technology, Hong Kong, China; Sida Peng, pengside@zju.edu.cn, Zhejiang University, Hangzhou, China; Jiaming Sun, suenjiaming@gmail.com, Zhejiang University, Hangzhou, China; Hujun Bao, bao@cad.zju.edu.cn, State Key Lab of CAD&CG, Zhejiang University, Hangzhou, China; Xiaowei Zhou, xwzhou@zju.edu.cn, State Key Lab of CAD&CG, Zhejiang University, Hangzhou, China.

Permission to make digital or hard copies of all or part of this work for personal or classroom use is granted without fee provided that copies are not made or distributed for profit or commercial advantage and that copies bear this notice and the full citation on the first page. Copyrights for components of this work owned by others than the author(s) must be honored. Abstracting with credit is permitted. To copy otherwise, or republish, to post on servers or to redistribute to lists, requires prior specific permission and/or a fee. Request permissions from permissions@acm.org.

methods leverage powerful 4D representations, like feature grids or point cloud sequences, to achieve high-quality rendering results. However, they are typically limited to short (1~2s) video clips and often suffer from large memory footprints when dealing with longer videos. To solve this issue, we propose a novel 4D representation, named Temporal Gaussian Hierarchy, to compactly model long volumetric videos. Our key observation is that there are generally various degrees of temporal redundancy in dynamic scenes, which consist of areas changing at different speeds. Motivated by this, our approach builds a multi-level hierarchy of 4D Gaussian primitives, where each level separately describes scene regions with different degrees of content change, and adaptively shares Gaussian primitives to represent unchanged scene content over different temporal segments, thus effectively reducing the number of Gaussian primitives. In addition, the tree-like structure of the Gaussian hierarchy allows us to efficiently represent the scene at

© 2024 Copyright held by the owner/author(s). Publication rights licensed to ACM.
0730-0301/2024/12-ART171 \$15.00
<https://doi.org/10.1145/3687919>

a particular moment with a subset of Gaussian primitives, leading to nearly constant GPU memory usage during the training or rendering regardless of the video length. Moreover, we design a Compact Appearance Model that mixes diffuse and view-dependent Gaussians to further minimize the model size while maintaining the rendering quality. We also develop a rasterization pipeline of Gaussian primitives based on the hardware-accelerated technique to improve rendering speed. Extensive experimental results demonstrate the superiority of our method over alternative methods in terms of training cost, rendering speed, and storage usage. To our knowledge, this work is the first approach capable of efficiently handling minutes of volumetric video data while maintaining state-of-the-art rendering quality.

CCS Concepts: • **Computing methodologies** → **Image-based rendering**.

Additional Key Words and Phrases: Novel view synthesis, neural rendering, neural radiance field, 3D Gaussian splatting

ACM Reference Format:

Zhen Xu, Yinghao Xu, Zhiyuan Yu, Sida Peng, Jiaming Sun, Hujun Bao, and Xiaowei Zhou. 2024. Representing Long Volumetric Video with Temporal Gaussian Hierarchy. *ACM Trans. Graph.* 43, 6, Article 171 (December 2024), 18 pages. <https://doi.org/10.1145/3687919>

1 INTRODUCTION

Volumetric videos aim to capture dynamic scenes from multiple viewpoints and provide the capability for free-viewpoint synthesis, enabling users to interact with virtual objects or characters for an immersive experience. The availability of high-quality volumetric videos is crucial in many domains including AR/VR, gaming, telepresence, and others. Although traditional volumetric video systems [Collet et al. 2015; Wu et al. 2020] have shown impressive results, they typically require bespoke hardware and sophisticated studio setup, which limits their accessibility and practicality.

Emerging neural rendering methods offer the ability to perform photorealistic view synthesis of dynamic scenes based on implicit or explicit 4D representations. Early work [Li et al. 2022; Pumarola et al. 2021a] aims to utilize neural radiance fields with temporal embeddings to parameterize dynamic scenes. Despite its storage-friendly model size, this representation has limited representation power and efficiency, leading to low-quality renderings that take several seconds or even minutes per frame. Recent research [Cao and Johnson 2023; Fridovich-Keil et al. 2023; Wang et al. 2022; Xu et al. 2024b] employs more powerful 4D representations, either through feature grids or point cloud sequences, to enhance rendering fidelity or efficiency. However, these methods generally only operate on short volumetric video sequences (1~2s) [Xu et al. 2024b; Yang et al. 2023b]. When applied to longer videos (1~10minutes), these approaches require very large models, posing scaling challenges considering practical storage size constraints.

In this paper, we introduce Temporal Gaussian Hierarchy, a novel 4D representation for compact modeling of long volumetric videos, while being efficient in training and rendering. Our key observation is that dynamic scenes generally consist of areas that change slowly and areas that change quickly, reflecting varying degrees of temporal redundancy. Motivated by this observation, our approach builds a multi-level hierarchy of scene primitives, e.g., 3D or 4D Gaussian splats [Kerbl et al. 2023; Yang et al. 2023b], to represent 4D scenes, where different levels model areas with different degrees of content change, and assign different numbers of scene primitives

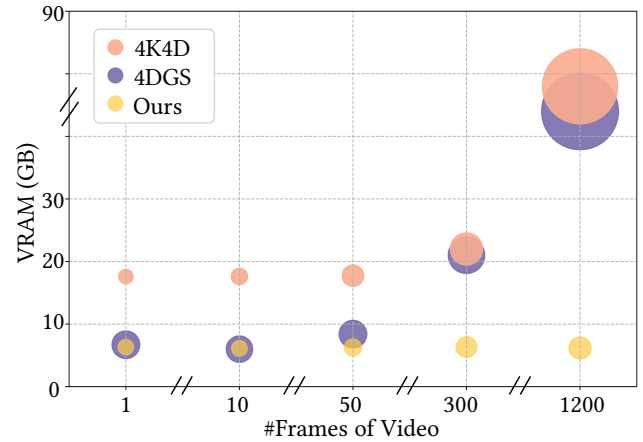


Fig. 2. **Training cost v.s. number of video frames.** By varying the number of video frames, we compare our method with recent state-of-the-art volumetric video techniques on the Neural3DV [Li et al. 2022] dataset in terms of training cost and storage usage, measured using VRAM (GB) and model size (MB), respectively. Each bubble’s area is proportional to its storage usage. Our method consistently maintains a constant training cost and near-constant storage usage regardless of the video frame length, demonstrating the scalability of our method for very long volumetric videos.

to each level, aiming to handle the temporal redundancy explicitly. Specifically, as illustrated in Fig. 3, the proposed hierarchical representation consists of multiple levels, and each level contains a set of segments responsible for modeling scenes within different temporal scales. Within each segment, we utilize a set of 4D Gaussian primitives [Yang et al. 2023b] to represent the scene, considering their high representation capability and rendering speed. Our experimental results demonstrate that in the proposed hierarchy, scene areas with slower motions generally share Gaussian primitives within segments across longer temporal scales, thereby reducing the number of scene primitives and leading to a decrease in model size. Moreover, the temporal Gaussian hierarchy allows us to represent the scene at a time step with a subset of segments instead of all Gaussian primitives, thus further reducing runtime memory.

Another advantage of temporal Gaussian hierarchy is that it enables us to keep efficient training and rendering regardless of the length of volumetric videos. The tree-like structure of our representation can efficiently locate the segments corresponding to a particular moment. Therefore, we can store the Gaussian hierarchy in random-access memory, and load the corresponding blocks into the GPU memory during the training or rendering of a scene at a specific moment. This strategy ensures that the GPU memory usage during runtime remains constant, regardless of the length of the volumetric video, guaranteeing efficient training and rendering.

To further reduce the model size of the volumetric video, we introduce a hybrid appearance model that consists of diffuse Gaussians and view-dependent Gaussians, which adaptively assigns the representational power to different areas of target scenes. This strategy can also mitigate the overfitting problems of Gaussian primitives while preserving the high capability of modeling dynamic

view-dependent appearance. Lastly, we develop a GPU-accelerated algorithm and hardware-accelerated rasterization pipeline for our representation to greatly enhance the **rendering speed**. As illustrated in Fig. 1, our method significantly surpasses previous methods in terms of training cost, rendering efficiency, and storage overhead, while achieving superior rendering quality.

We evaluate our method across various widely used datasets for dynamic view synthesis given multi-view input. Additionally, we collect a set of long multi-view sequences (5-10 minutes) to demonstrate the scalability of our method on video length. Both qualitative and quantitative results demonstrate that our method outperforms existing baselines, showcasing state-of-the-art visual quality and rendering speed while requiring significantly less training cost and memory usage, enabling the reconstruction and rendering of long volumetric videos. Using an RTX 4090 GPU, our method can process videos with 18,000 frames at a 1080p resolution, achieving a rendering speed of 450 FPS. We also collect a long real-world multi-view dataset, dubbed *SelfCap*, to validate our method.

Our contributions can be summarized as follows:

- We introduce a novel, efficient, and expressive Temporal Gaussian Hierarchy representation for long volumetric video. To our knowledge, our method is the first approach capable of handling minutes of volumetric video data.
- We propose a Compact Appearance Model and a new rasterization implementation to facilitate real-time and high-quality dynamic view synthesis while maintaining a compact size.
- We propose a system to efficiently model long volumetric videos for the first time and demonstrate state-of-the-art dynamic view synthesis quality on the *Neural3DV* [Li et al. 2022], *ENeRF-Outdoor* [Lin et al. 2022] and *MobileStage* [Xu et al. 2024b] datasets, while also achieving the best rendering speed with reduced training cost and memory usage.

2 RELATED WORK

2.1 Volumetric Videos

Volumetric videos capture dynamic scenes from multiple viewpoints and provide the capability for immersive free-viewpoint synthesis. Earlier works leverage template-priors like shape-from-silhouettes [Ahmed et al. 2008], deformable models [Carranza et al. 2003] and template-free dynamic reconstruction systems with depth sensor integration [Newcombe et al. 2015]. Some research explores fusion methodologies, incorporating priors like skeletal structures and parametric body shapes to facilitate non-rigid 3D reconstruction, as seen in the works of [Yu et al. 2017, 2018]. Another research line explores data-driven approaches [Bozic et al. 2020] for dynamic 3D reconstruction beyond photometric consistency criteria, with works like [Lombardi et al. 2019] introducing generative models for more flexible reconstruction frameworks. These methods either cannot be applied to complex scenes with many occlusions, require parameterized templates, or rely on expensive and hardware-intensive capture devices, all of which limit the application of volumetric video in real-world scenarios.

2.2 Neural Scene Representations for Dynamic Scenes

Neural scene representations have attracted significant attention from the research community due to their impressive performance in 3D reconstruction and novel-view synthesis. Methods such as NeRF [Mildenhall et al. 2021], SDF [Park et al. 2019], and OCC-Net [Mescheder et al. 2019] parameterize scenes as radiance fields, signed distance functions, and occupancy using neural networks. However, these techniques struggle to generalize to dynamic scenes, because of the illumination variations and complex object motions.

Recent advancements [Fang et al. 2022; Park et al. 2021a,b; Pumarola et al. 2021b; Tretschk et al. 2021a] have seen efforts to extend NeRF into volumetric videos for dynamic view synthesis. Some approaches model dynamic scenes [Park et al. 2021a,b; Pumarola et al. 2021b] by learning a canonical static template with deformable fields represented by spatial offsets. Yet, these methods can only handle limited camera changes and object motions. Some approaches [Du et al. 2021] directly employ 4D NeRF, incorporating timestamps along with spatial location and view direction to address spatial changes. To enhance rendering quality, other works explore hybrid representations [Cao and Johnson 2023; Fridovich-Keil et al. 2023; Xu et al. 2024b] to parameterize dynamic scenes. However, these approaches often incur substantial computational costs for training and storage, limiting their practicality and quality. Alternatively, some methods [Chen et al. 2021; Li et al. 2023; Long et al. 2022; Wang et al. 2021; Yu et al. 2021] aim to construct feed-forward models for inferring 3D NeRF from multi-view images, thereby extending their applicability to dynamic scenes. However, due to the lack of temporal modeling and the computational overhead of convolution operations in image encoders, these methods suffer from the low-quality renderings and slow rendering speeds, especially for long volumetric videos.

To accelerate NeRF rendering, several approaches utilize explicit structures, employing shallow MLPs to represent scenes. These include voxel grids [Fridovich-Keil et al. 2022; Garbin et al. 2021; Hedman et al. 2021; Müller et al. 2022], surfaces [Chen et al. 2023; Hasselgren et al. 2022; Kulhanek and Sattler 2023; Lu et al. 2023], and point-based representations [Aliev et al. 2020; Lassner and Zollhofer 2021; Rakhimov et al. 2022; Rückert et al. 2022]. While these methods significantly reduce the computational load of neural network evaluations for rendering, they often incur additional storage consumption. To mitigate memory costs, recent efforts have explored weight decomposition techniques [Chen et al. 2022; Takikawa et al. 2022; Tang et al. 2022], while limiting their capacity to represent dynamic scenes effectively. Some methods [Park et al. 2021b; Tretschk et al. 2021b; Wang et al. 2022] have also proposed dynamic modeling on sparse voxel grids and deformable fields for videos, showing promise for short videos but introducing storage overhead when applied to longer volumetric sequences. In contrast, our proposed approach introduces an efficient and compact Temporal Gaussian Hierarchy for dynamic view synthesis. This framework facilitates scalability to high-resolution and extensive volumetric videos while maintaining real-time rendering speeds.

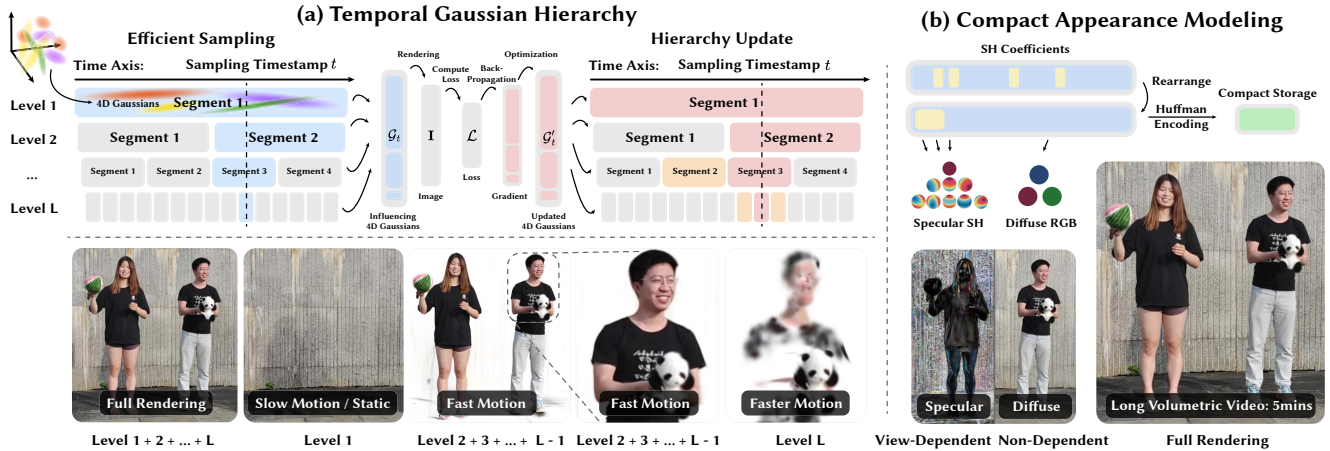


Fig. 3. **Overview of our framework.** Given a long multi-view video sequence, our method can generate a compact volumetric video with minimal training and memory usage while maintaining real-time rendering with state-of-the-art quality. (a) We propose a hierarchical structure where each level consists of multiple temporal segments. Each segment stores a set of 4D Gaussians [Yang et al. 2023b] to parametrize scenes. As shown at the bottom, the 4D Gaussians in different segments represent different granularities of motions, efficiently and effectively modeling video dynamics. (b) The appearance model leverages gradient thresholding to obtain sparse Spherical Harmonics coefficients, resulting in very compact storage while still maintaining view-dependent effects well.

2.3 Gaussian Splatting for Dynamic Scenes

3D Gaussians [Kerbl et al. 2023] have become widely popular due to their capacity for efficiently reconstructing high-fidelity 3D scenes from posed images. In order to adapt 3D Gaussians for dynamic scenes, Dy3DGS [Luiten et al. 2024] first proposes to reconstruct dynamic scenes by tracking 3D Gaussians on a frame-by-frame basis. However, their approach leads to large models for long sequences since they need to store the per-point transform information for every frame. In comparison, our method takes advantage of the different degrees of temporal redundancy by using segments of varying lengths at different levels, sharing temporal information across frames to maintain a low disk storage overhead. Dynamic-Gaussian [Lu et al. 2024; Yang et al. 2023a] proposes learning the temporal motion and rotation of each 3D Gaussian, thereby supporting dynamic tracking applications. Some studies utilize more powerful modules [Wu et al. 2023b] like MLP to predict temporal motion or integrate dynamic Gaussians into monocular videos [Yang et al. 2023a] or human avatar animations [Jung et al. 2023]. However, it is very challenging to parameterize very sudden motions on dynamic objects.

Another line of research leverages 4D Gaussians [Duan et al. 2024; Lin et al. 2023a; Yang et al. 2023b] to model 3D dynamics. These studies propose to learn high-dimensional rotations along the time axis and utilize marginal observations at specific timesteps to derive the 3D Gaussian for fast rendering. Many works leverage this underlying representation for 4D generation [Ling et al. 2023; Ren et al. 2023]. However, these frameworks incur significant computational overhead such as VRAM and storage when processing extensive video data. For example, 4DGS [Yang et al. 2023b] requires to render a scene at a particular moment with all Gaussian primitives across the whole temporal scale, which can easily lead to the VRAM exhaustion. In contrast, our proposed Temporal Gaussian Hierarchy allows using a particular set of 4D Gaussians [Yang et al. 2023b] to describe

the content of dynamic scenes within the corresponding segment. Thanks to this design, our model maintains nearly constant memory costs for both training and inference, along with compact storage. This feature enables our method to scale effectively to very long volumetric videos for dynamic view synthesis.

3 METHOD

3.1 Overview

Given multi-view videos, our goal is to efficiently reconstruct a corresponding compact and lightweight 4D volumetric representation that can be played back in real-time. To achieve this goal, we first develop a novel 4D representation, dubbed Temporal Gaussian Hierarchy, for efficiently modeling the different scales of motion and dynamics in a long dynamic scene (Sec. 3.2). Then, we propose a compact appearance representation (Sec. 3.3), where only the few view-dependent points are modeled using all degrees of Spherical Harmonics [Müller 2006] to greatly reduce the storage cost for representing long volumetric videos while maintaining the rendering quality. Finally, we develop an efficient rendering pipeline with hardware-accelerated rasterization and precomputation for rendering TGH in real-time (Sec. 3.5). An overview of the proposed method can be found in Fig. 3.

3.2 Temporal Gaussian Hierarchy

Previous methods for volumetric videos [Lin et al. 2023b; Xu et al. 2024b; Yang et al. 2023b] require significant GPU memory and time, both of which typically scale with the duration of the video, limiting their applicability to representing long volumetric videos. To overcome these problems, we design a novel 4D representation, Temporal Gaussian Hierarchy. By leveraging a tree-like structure to manage hierarchical temporal segments for different motion granularities, we can efficiently identify all relevant segments for a specific

timestamp and thus maintain a nearly-constant computation cost (VRAM and speed) for volumetric videos of arbitrary length.

3.2.1 Temporal Hierarchy Structure. Fig. 3(a) provides an structural overview of the Temporal Gaussian Hierarchy. Dynamic scenes typically encompass regions with varying scales of motion. We represent this diversity using Temporal Gaussian Hierarchy. Concretely, we construct a hierarchical structure in which each level accommodates many temporal segments of equal length. The segment length at deeper levels is half that of the preceding layer. We denote the total duration of the video as T , the depth of hierarchy structure is L and the segment length at the root level as S . So the temporal scale of segments s_l and the number of segments N_l at level l can be expressed as:

$$s_l = \frac{S}{2^l}, \quad (1)$$

$$N_l = \text{ceil}\left(\frac{T}{s_l}\right), \quad (2)$$

where ceil denotes rounding up to the closest integer. In addition, we append a single global segment with a length of ∞ to capture static part of the scene.

In each segment, we store a set of 4D Gaussians (4DGS) [Yang et al. 2023b] to represent the dynamic scenes. Specifically, 4D Gaussian is defined with 4D means $\boldsymbol{\mu} \in \mathbb{R}^4$, 4D scaling $\mathbf{s} \in \mathbb{R}^4$, a scalar opacity $o \in \mathbb{R}$ and two isotropic left and right quaternions $\mathbf{q}_l \in \mathbb{R}^4$, $\mathbf{q}_r \in \mathbb{R}^4$, base color $\mathbf{c}_{base} \in \mathbb{R}^3$, and residual spherical harmonics (SH) coefficients $\mathbf{h} \in \mathbb{R}^m$ with m denoting the number of SH bases. The 4D covariance matrix of the Gaussian distribution is defined as:

$$\Sigma = \mathbf{R} \mathbf{S} \mathbf{S}^T \mathbf{R}^T, \quad (3)$$

where \mathbf{S} is a diagonal matrix with \mathbf{s} as its diagonal elements, and \mathbf{R} is the symmetric expansion of the two isotropic quaternions. The opacity of the 4D Gaussians follows a Gaussian distribution $o_t \sim \mathcal{N}(t; \mu_t, \sigma_t)$ around its temporal center μ_t , with a scale characterized by the last element of the 4D covariance matrix $\sigma_t = \Sigma_{4,4}$ [Yang et al. 2023b]. Considering the temporal range where the Gaussian opacity is larger than a small value o_{th} , we can compute the influence radius r and influence range $[\bar{\tau}, \underline{\tau}]$ of the Gaussian by inversely evaluating the function of the Gaussian distribution $\mathcal{N}(t; \mu_t, \sigma_t)$ using:

$$r = \text{sqrt}\left(\frac{\log(o_{th})}{-0.5} \cdot \sigma_t\right), \quad (4)$$

$$\bar{\tau} = \mu_t - r, \quad \underline{\tau} = \mu_t + r.$$

Temporal Gaussian Hierarchy is designed to model video dynamics efficiently and effectively: long segments at a coarse level work well for slow motions, while short segments at a finer level are better for fast motions. To achieve this, when placing the 4D Gaussians in the hierarchical structure, we need to ensure the range of the segment covers the Gaussians influence radius within it and can't be covered by any segments in next levels. Specifically, we first calculate the start $\bar{\tau}_{l,n}$ and end $\underline{\tau}_{l,n}$ timestamp of the n -th segment at level l with temporal scale s_l :

$$\bar{\tau}_{l,n} = n \cdot s_l, \quad \underline{\tau}_{l,n} = (n+1) \cdot s_l, \quad (5)$$

and then use the following strategy to place the 4D Gaussians in the structure:

$$\begin{aligned} \bar{\tau}_{l+0,n} \leq \bar{\tau} \leq \underline{\tau} \leq \underline{\tau}_{l+0,n}, \\ \forall m \in \{1, 2, \dots, M\}, \bar{\tau}_{l+1,m} > \bar{\tau} \vee \underline{\tau} > \underline{\tau}_{l+1,m}, \end{aligned} \quad (6)$$

where $m \in \{1, 2, \dots, M\}$ denotes all segment indices and M denotes the number of segments in the next level $l+1$. This makes the Temporal Gaussian Hierarchy structure unique and make sure that each 4D Gaussian is placed in the shortest possible segment.

3.2.2 Efficient Rendering. With the Temporal Gaussian Hierarchy, we can efficiently sample the 4D Gaussians that influence this timestamp t to render images. Since the segments at each level don't overlap, the timestamp is influenced by only one segment at level l , and the corresponding index n_l^t is:

$$n_l^t = \text{floor}\left(\frac{t}{s_l}\right), \quad (7)$$

resulting in L segments across all levels. The computational complexity of this identification process is $O(\log N)$, where N is the total number of segments in the hierarchy. We then concatenate all 4D Gaussians within the influenced segments with index $\{n_l^t | l \in 1 \dots L\}$ to obtain the streaming Gaussians \mathcal{G}_t and render the images with a differentiable rasterizer.

In practice, we place the Temporal Gaussian Hierarchy structure inside RAM and only copy the influenced segments to the GPU memory. This helps save a significant amount of GPU memory and maintains near-constant GPU memory usage regardless of the length of the volumetric video, whereas naive 4DGS, which computes the temporal range for all 4D Gaussians, incurs large GPU memory usage with poor sampling efficiency for long video data. Moreover, there is no speed downgrade for rendering because this memory copying process can be parallelized with the rendering.

Because the segment lengths of adjacent levels have an integer ratio, segments at different levels often have the same starting time. This could result in increased usage of GPU memory during rendering. In this case, many 4D Gaussians with short influence radius can span two adjacent segments across many levels. According to Eq. (6), this tends to make the Gaussian appear in the longer segments, which in turn raises its probability of being sampled for rendering at many timestamps, leading to an increase in GPU memory usage.

To solve this issue, we propose a corrected offset $\bar{\tau}_l$ of level l by half of the segment length of the next level at different levels to avoid these situations:

$$\bar{\tau}_l = -\frac{S}{2^{l+2}}, \quad (8)$$

With this corrected offset, the start and end timestamp of Eq. (5) and the index n^t of Eq. (7) can be rewritten as:

$$\bar{\tau}_{l,n} = \bar{\tau}_l + n \cdot s_l, \quad \underline{\tau}_{l,n} = \bar{\tau}_l + (n+1) \cdot s_l, \quad (9)$$

$$n_l^t = \text{floor}\left(\frac{t - \bar{\tau}_l}{s_l}\right). \quad (10)$$

3.2.3 Hierarchy Update. After each training step, the properties of the streaming Gaussians \mathcal{G}_t are optimized with the reconstruction loss, resulting in an updated set \mathcal{G}'_t with varying influence radius as reflected by Eq. (4). So it is necessary to reassign the optimized

4D Gaussians back into their respective levels and nodes in the hierarchical structure using Eq. (6).

Specifically, for the updated Gaussian with a new opacity distribution $o'_l \sim \mathcal{N}(t; \mu'_l, \sigma'_l)$, the influence range $[\bar{\tau}', \underline{\tau}']$ can be computed using Eq. (4), with the same opacity threshold o_{th} . Subsequently, the corresponding indices $\bar{n}'_l, \underline{n}'_l$ for the start and end influence timestamps $\bar{\tau}', \underline{\tau}'$ are computed for each level of the Gaussian hierarchy using Eq. (10). We can determine whether the Gaussian can adapt to this level l by comparing whether \bar{n}'_l equals \underline{n}'_l . Then, the updated level l' is defined to be the maximum level satisfying this condition. Note that since our update algorithm operates on levels instead of individual segments, the computational complexity remains $O(L)$, where L is the total number of levels in the hierarchy as defined in Sec. 3.2. Since L is a constant with respect to the length of the represented volumetric video, this helps maintain the constant memory usage and iteration speed of our method.

3.3 Compact Appearance Model

Original 3DGS [Kerbl et al. 2023] utilizes standard spherical harmonics (SH) evaluation, denoted as $\text{evalSH}(\cdot)$, to obtain the view-dependent color $\mathbf{c} = \mathbf{c}_{base} + \text{evalSH}(\mathbf{h}, \mathbf{d})$, where $\mathbf{h} \in \mathbb{R}^m$ represents the residual SH coefficients with m denoting the number of SH bases, \mathbf{d} denotes the view direction and \mathbf{c}_{base} is the 3-channel base color of the Gaussian, resulting in a total of $3 \times (m + 1)^2$ parameters for appearance per Gaussian. However, the large number of bases m in standard SH representation results in significant storage overhead, particularly when scaling to long videos.

To address this issue, we propose a Compact Appearance Model that leverages sparse SH to efficiently capture view-dependent effects with a reduced model size while maintaining comparable rendering quality to the full-SH model. The diffuse part of the volumetric video does not necessarily require high-degree SH for accurate modeling, inspiring us to exclude this type of Gaussians to reduce the storage. Intuitively, diffuse Gaussians should receive a low magnitude gradient on its residual SH coefficients \mathbf{h} even when they are rendered and optimized as view-dependent ones. Thus we can use a zero-initialization and gradient thresholding strategy to successfully identify these Gaussians and retain their diffuse properties. Specifically, we first initialize the residual SH coefficients \mathbf{h} of all Gaussians with zeros. Then, a gradient threshold g_{th} is defined to modify the gradient values of the low-magnitude ones $\|\mathbf{g}_h\|_2 < g_{th}$ as zero. For the view-dependent Gaussians, we optimize them regardless of their gradient scale to enable our model to express view-dependent effects. This process can be described using:

$$\mathbf{g}'_h = \begin{cases} \mathbf{g}_h, & \|\mathbf{g}_h\|_2 \geq g_{th} \vee \|\mathbf{h}\|_2 \neq 0 \\ 0, & \|\mathbf{g}_h\|_2 < g_{th} \wedge \|\mathbf{h}\|_2 = 0 \end{cases}. \quad (11)$$

To regulate the number of view-dependent Gaussians, we additionally compute its proportion and set the gradient threshold g_{th} to infinity for future optimization steps once the proportion reaches a certain ratio λ_h .

After training, we group the 4D Gaussians according to whether they are diffuse or view-dependent. This ensures that all zeros in the SH coefficients of all points C_d can be grouped together before being fed into the Huffman Coding algorithm [Huffman 1952], further boosting the compression ratio.

3.4 Training

Given the rendered image \mathbf{I} and ground-truth image \mathbf{I}_{gt} , we optimize our model with the following objective:

$$\mathcal{L} = \lambda_m \cdot \mathcal{L}_{mse} + \lambda_s \cdot \mathcal{L}_{ssim} + \lambda_p \cdot \mathcal{L}_{perc}, \quad (12)$$

where \mathcal{L}_{mse} denotes the mean squared error using

$$\mathcal{L}_{mse} = \|\mathbf{I} - \mathbf{I}_{gt}\|_2^2, \quad (13)$$

\mathcal{L}_{ssim} denotes the structural similarity [Wang et al. 2004a] error

$$\mathcal{L}_{ssim} = 1 - \text{SSIM}(\mathbf{I}, \mathbf{I}_{gt}), \quad (14)$$

and \mathcal{L}_{perc} denotes the perceptual similarity [Zhang et al. 2018a] loss by computing the L_1 difference between the extracted features with AlexNet [Krizhevsky et al. 2012] (denoted by Φ):

$$\mathcal{L}_{perc} = \|\Phi(\mathbf{I}) - \Phi(\mathbf{I}_{gt})\|_1. \quad (15)$$

λ_m, λ_s and λ_p are loss weights of $\mathcal{L}_{mse}, \mathcal{L}_{ssim}$ and \mathcal{L}_{perc} . Following 3DGS [Kerbl et al. 2023], we also apply the adaptive control scheme to split, clone and prune the 4D Gaussian ellipsoids every 100 iterations using their strategy. These newly split and cloned ellipsoids can be easily updated into Temporal Gaussian Hierarchy using the algorithm described in Sec. 3.2. More details can be found in *Supplemental Material*.

3.5 Real-Time Rendering

To facilitate optimization of the Gaussians, 3DGS [Kerbl et al. 2023] developed a CUDA-based software rasterizer for their Gaussian Splatting algorithm. To further improve the rendering speed during inference, we develop a new hardware-accelerated rasterization algorithm that combines CUDA-based sorting and Graphics-based rasterization to replace the standard software rasterizer.

Given the timestamp t , we acquire the streaming Gaussians set \mathcal{G}_t using Eq. (7) and arrange them in back-to-front order based on view-space depth with a fast radix sort on the GPU [Paszke et al. 2019]. These sorted Gaussians are then transferred to the hardware rasterizer [Shreiner et al. 2009] and projected into screen space using the 3D Gaussian Splatting algorithm, resulting in 2D Gaussians. Since 2D Gaussians are not directly recognized by the rasterizer for computing gaussian-pixel pairs, we transform the 2D Gaussian into a 2D rectangular primitive (quad) with opacity thresholding [Kopanas et al. 2024; mkkellogg 2024]. The hardware rasterization pipeline [Shreiner et al. 2009] then rasterizes the set of quads onto the screen, generating quad-pixel pairs (fragments) in which we can easily compute the opacity and color for the pixel locations by evaluating the multivariant Gaussian distribution function. Since the Gaussians are sorted in back-to-front order, the hardware rasterizer can efficiently perform back-to-front alpha blending [Mildenhall et al. 2021] on all fragments corresponding to a particular pixel to compute its final color, which is concatenated to be the final rendered image. By directly utilizing the hardware rasterization pipeline and using the GPU for sorting, this implementation can lead to better utilization of the GPU and lead to a significant improvement in rendering efficiency. As demonstrated in Fig. 8, our approach achieves a 5x speed improvement over the standard software rasterization process [Kerbl et al. 2023]. The implementation is open-sourced at <https://github.com/dendenxu/fast-gaussian-rasterization>.



Fig. 4. **Qualitative comparisons on Mobile-Stage [Xu et al. 2024b] with 1600 frames.** For long videos of 1200 frames, our model can be directly trained on the whole sequence and only requires 10.2GB of VRAM for training and 0.42GB of storage, which is 2x and 4x less, respectively, compared to the second smallest implicit method, ENeRF [Lin et al. 2022]. Contrarily, 4K4D [Xu et al. 2024b] and 4DGS [Yang et al. 2023b] could only be trained on small segments of 300 frames without encountering Out-of-Memory error. Our model achieves high rendering quality and can be rendered at 440 FPS.

4 IMPLEMENTATION DETAILS

Optimization. Our TGH representation is trained using the PyTorch framework [Paszke et al. 2019; Xu et al. 2023] along with custom CUDA [Sanders and Kandrot 2010] kernels for efficient update of the Temporal Gaussian Hierarchy structure. We optimize the model using an Adam [Kingma and Ba 2014] optimizer with a

learning rate of $1.6e^{-4}$ following 3DGS [Kerbl et al. 2023]. Typically, a model is trained for 50k iterations for a sequence length of 1200 frames, which takes around 2 hours on an RTX 4090 GPU. We scale the number of iterations linearly with the sequence length. Notably, different datasets come in different resolutions, thus the speed for an iteration might vary accordingly, leading to varying training times. Following 3DGS [Kerbl et al. 2023] and 4DGS [Yang et al. 2023b],



Fig. 5. **Qualitative comparisons on Neural3DV [Li et al. 2022] with 1200 frames.** Our method can not only recover high-frequency details of dynamic objects but also maintain the sharp appearance of the background with low training costs and a compact model size. 4K4D [Xu et al. 2024b] and 4DGS [Yang et al. 2023b] could only be trained on small segments of 300 frames due to VRAM limitation.

we perform adaptive control on the number of Gaussians by splitting, cloning, and pruning the Gaussians based on their view-space gradients and opacity values every 100 iterations. Thanks to our efficient Temporal Gaussian Hierarchy structure, this adaptive control

can be limited to only the sampled segments during the previous iterations, which significantly lower the GPU memory usage and computational cost for this stage.

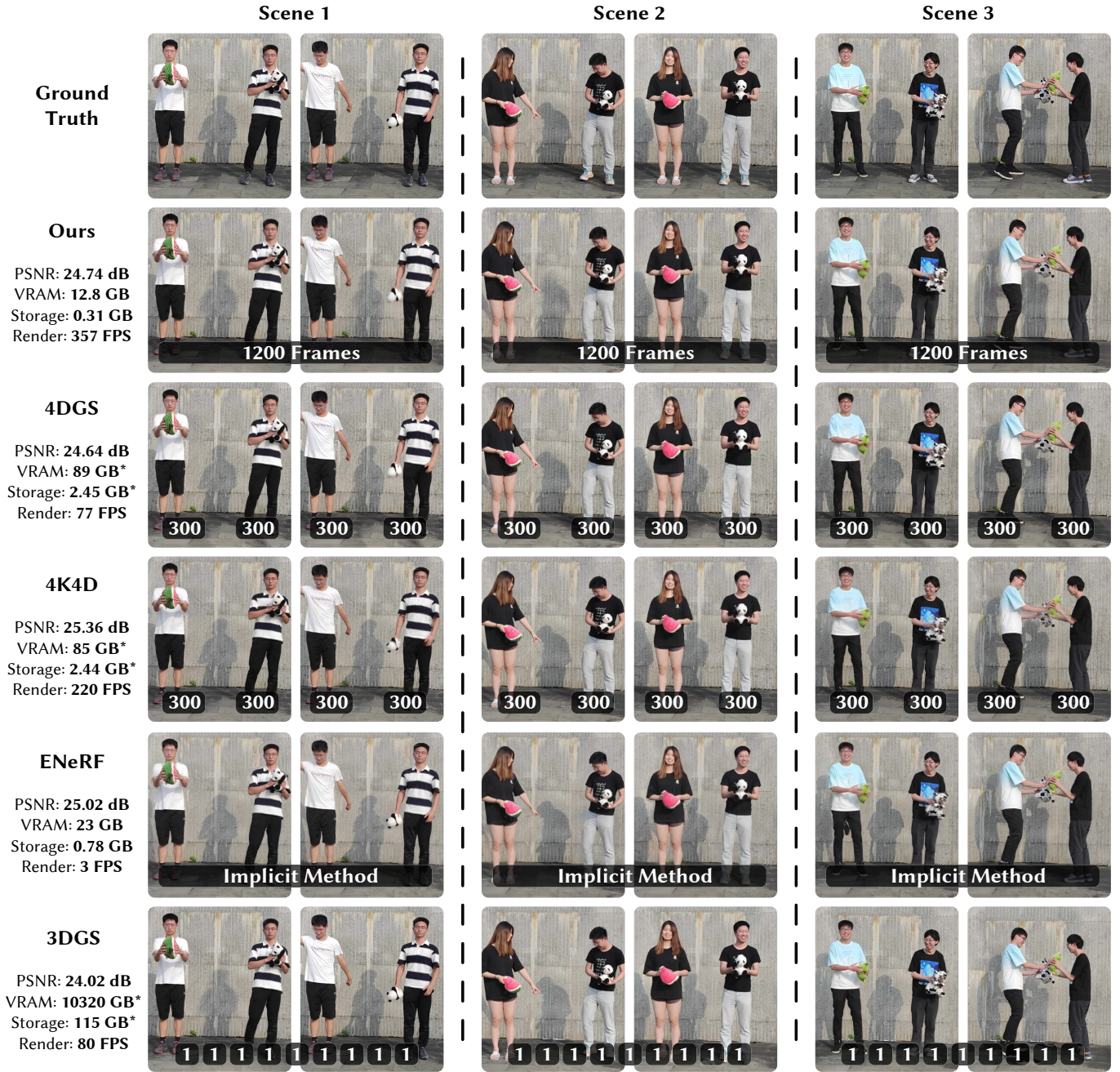


Fig. 6. **Qualitative comparisons on ENeRF-Outdoor [Lin et al. 2022] with 1200 frames.** Here we show multiple sequences for comparison. Our method achieves high-quality rendering while using only 50% of the VRAM and 40% of the storage required by ENeRF, and it is 1.6x faster than the second best method, 4K4D. Note that 4K4D [Xu et al. 2024b] and 4DGS [Yang et al. 2023b] encounters Out-of-Memory error for sequences longer than 300 frames.

Hyperparameters. Hyperparameters of the Temporal Gaussian Hierarchy structure and the Compact Appearance model are set empirically according to the sensitivity analysis in Sec. 5.4 or directly followed from previous work. Specifically, the number of levels L in the Temporal Gaussian Hierarchy structure is set to 9 and the

root segment S size is set to 10s throughout evaluation. Following 4DGS [Yang et al. 2023b], the opacity threshold for the marginal temporal Gaussian o_{th} is set to 0.05. For the Compact Appearance model, we set the gradient threshold g_{th} for separating diffuse and view-dependent Gaussians to $1.0e^{-6}$ and the cut-off ratio λ_h to 0.15.

Similar to 3DGS [Kerbl et al. 2023], we use 3 degrees of Spherical Harmonics for the view-dependency modeling, resulting in $m = 48$ SH basis functions. The weights for the mean squared error and structure and perceptual similarity loss $\lambda_m, \lambda_s, \lambda_p$ are empirically set to 0.8, 0.2, and 0.01, respectively.

Initialization. Following 3DGS [Kerbl et al. 2023], we use the sparse point clouds output by the SfM process [Schonberger and Frahm 2016] for every frame of the volumetric video for initialization. For methods utilizing a different initialization strategy [Xu et al. 2024b; Yang et al. 2023b], we adapt their initial number of points to be at least as large as ours by upsampling their initial point clouds to ensure a fair comparison. The initial 3D scaling $s_{x,y,z}$ of the Gaussians is determined by performing a KNN sampling on the sparse point cloud and computing the average distances following 3DGS [Kerbl et al. 2023]. The temporal scaling is s_t is set to frame the time of the sequence to be reconstructed.

5 EXPERIMENTS

5.1 Settings

5.1.1 Datasets. We use public datasets *Neural3DV* [Li et al. 2022], *ENeRF-Outdoor* [Lin et al. 2022], *MobileStage* [Xu et al. 2024a,b] and *CMU-Panoptic* [Joo et al. 2015] for evaluation, since they provide longer video sequences. *Neural3DV* is a popular benchmark for novel view synthesis. It is captured by a multi-view system with 19-21 cameras. The videos are recorded at a resolution of 2704×2028 and 30FPS. We select the *flame_salmon* scene for evaluation, which uses 19 cameras and contains 1200 frames in total. In line with prior work, we downsample the videos by a factor of two and follow the training and testing camera split as specified by [Li et al. 2022]. *ENeRF-Outdoor* is a dynamic dataset of outdoor scenes, collected by 18 synchronized cameras at 1920×1080 and 60FPS. We select three 1200-frame sequences for evaluation: *actor1_4*, *actor2_3* and *actor5_6*. Each sequence contains two actors holding objects in an outdoor environment. We use the ‘08’ camera as the testing view and the remaining views as the training views. *MobileStage* is a multi-view dataset focused on dynamic humans. The dataset records actors at 30FPS with 24 1080p cameras. We evaluate on the *dance3* sequence, which captures 3 dancing actors for 1600 frames. The ‘05’ camera is used for testing and the remaining cameras are for training. The dataset is challenging for dynamic view synthesis due to the complex motion and fast movement involved in dancing. *CMU-Panoptic* [Joo et al. 2015] is a large-scale multi-view dataset capturing varying everyday human interactions and activities. We follow Dy3DGS [Luiten et al. 2024] to select three subsequences from the *sports* clip, namely the *box*, *softball* and *basketball* subsequences, and also follow their training and testing split of 27 to 4. Contrary to Dy3DGS [Luiten et al. 2024], we use the full resolution of the 31 HD cameras and the full length of the clip, resulting in a resolution of 1080p and a length of 1000-frame, 800-frame and 700-frame respectively for the three subsequences.

In addition to leveraging existing public datasets, we build a new dynamic multi-view dataset named *SelfCap* to evaluate our approach. This dataset comprises three dynamic videos, each captured at 60FPS in 4K resolution using a synchronized array of 22 iPhone cameras. The videos in this dataset range from 2 to 10 minutes in

length, significantly surpassing the durations of previous datasets. By training and evaluating our methods on these long video sequences, we demonstrate our ability to efficiently represent long volumetric videos. We will publicly release this dataset to facilitate research on long volumetric video modeling.

All datasets are captured using synchronized static camera arrays, and no explicit temporal consistency is enforced other than sharing the camera parameters. The datasets mainly contain static backgrounds with dynamic foregrounds for everyday dynamic activities involving dynamic humans and objects that are mostly diffuse, which further justifies the use of the global segment and Compact Appearance model. Noticeably, our representation is defined on the world coordinate system, thus even if the cameras are moving, it should not have too much impact as long as the camera parameters are known.

5.1.2 Baselines. We include several state-of-the-art baseline methods for comparison, including 3DGS [Kerbl et al. 2023], 4DGS [Yang et al. 2023b], ENeRF [Lin et al. 2022], 4K4D [Xu et al. 2024b] and Dy3DGS [Luiten et al. 2024]. 3DGS employs explicit Gaussian primitives to effectively model 3D scenes. While this technique achieves high-quality rendering and impressive speed, its application is limited to static scenes. To extend its evaluation to dynamic scenes, we experiment with training 3DGS on a per-frame basis for the testing frames for comparison. Dy3DGS [Luiten et al. 2024] optimizes a per-frame tracking of the scene geometry and appearance using 3DGS [Kerbl et al. 2023] in a streaming fashion. 4DGS expands 3DGS along the temporal axis and introduces a 4D representation to capture the spatial-temporal dynamics. By leveraging 4D primitives that encompass both spatial and temporal dimensions, it enables explicit geometry and appearance modeling in volumetric videos. Besides the explicit approaches, we also consider dynamic approaches that utilize implicit and hybrid representations. ENeRF constructs a cascade cost volume to predict coarse scene geometry, which is then used to guide point sampling for generative implicit radiance fields. 4K4D integrates dynamic point clouds as input and designs a hybrid appearance model to improve rendering quality. Baseline models are trained with the official implementation at different frame-length settings. For 3DGS, we train it in a per-frame fashion. For 4DGS and 4K4D, we split each video into 4 equal-length segments, and trained them on each segment individually. As for ENeRF, we finetune the official pre-trained model on the whole video.

5.1.3 Metrics. We employ the PSNR, SSIM [Wang et al. 2004b], and LPIPS [Zhang et al. 2018b] metrics to assess the quality of rendered images in our methods and baselines. PSNR measures the l_2 difference between a reconstructed image and its ground truth, with higher values indicating less disparity. SSIM quantifies the structural similarity between images, with values ranging from -1 to 1, where higher values denote greater similarity. LPIPS evaluates perceptual similarity, aligned with human perception.

Besides, we consider VRAM, storage, training time, and rendering speed to illustrate training and inference costs. VRAM represents the GPU memory required for training, measured in gigabytes (GB). Storage indicates the model size on disk, measured in gigabytes (GB). Baseline methods such as 3DGS, 4K4D, and 4DGS are incapable of handling extensive volumetric videos. For comparison, we train

Table 1. **Quantitative comparison on *Neural3DV* [Li et al. 2022], *ENeRF-Outdoor* [Lin et al. 2022], *MobileStage* [Xu et al. 2024b] and *CMU-Panoptic* [Joo et al. 2015].** We report PSNR, SSIM, and LPIPS to evaluate rendering quality. VRAM and storage are used to assess the training and storage costs. "Train." and "Render." denote the training time and rendering FPS, respectively. Note that we highlight the best one for clarification. 4K4D, 4DGS and 3DGS could only be trained in 300-frame or 1-frame segments. "*" indicates that the computational costs for these methods are summed over the entire video. "***" indicates that the method uses the same Gaussian initialization as ours.

Metrics	Neural3DV [Li et al. 2022]						ENeRF-Outdoor [Lin et al. 2022]					MobileStage [Xu et al. 2024b]					CMU-Panoptic		
	Ours	4DGS	4K4D	ENeRF	3DGS	Dy3DGS	Ours	4DGS	4K4D	ENeRF	3DGS	Ours	4DGS	4DGS**	4K4D	ENeRF	3DGS	Ours	Dy3DGS
PSNR ↑	29.44	28.89	21.29	23.48	28.61	25.91	24.74	24.64	25.36	25.02	24.02	27.29	23.21	24.03	25.90	19.14	28.02	28.55	24.27
SSIM ↑	0.9450	0.9521	0.8266	0.8944	0.9498	0.8809	0.8392	0.7855	0.8080	0.7824	0.8231	0.9127	0.7876	0.8150	0.8788	0.7492	0.9172	0.9558	0.9432
LPIPS ↓	0.2144	0.1968	0.3715	0.2599	0.2103	0.2555	0.2624	0.3118	0.3795	0.3043	0.2765	0.2536	0.4209	0.3880	0.3872	0.4365	0.2383	0.4016	0.5135
VRAM ↓	6.1 GB	84 GB*	84 GB*	23 GB	7200 GB*	5.0 GB	12.8 GB	89 GB*	85 GB*	23 GB	10320 GB*	10.2 GB	92 GB*	88 GB*	88 GB*	22 GB	15200 GB*	10.0 GB	11.4 GB
Storage ↓	0.09 GB	2.68 GB*	2.46 GB*	0.83 GB	37.5 GB*	19.5 GB	0.31 GB	2.45 GB*	2.44 GB*	0.78 GB	115 GB*	0.42 GB	1.83 GB*	2.51 GB*	4.25 GB*	1.40 GB	106 GB*	0.22 GB	6.42 GB
Train. ↓	2.1 h	10.4 h*	26.6 h*	4.6 h	110 h*	37.1 h	4.4 h	12.7 h*	29.3 h*	6.5 h	280 h*	10.4 h	14.4 h*	12.7 h*	40.5 h*	6.1 h	213 h*	10.8 h	20.8 h
Render. ↑	550 FPS	90 FPS	290 FPS	5 FPS	150 FPS	610 FPS	357 FPS	77 FPS	220 FPS	3 FPS	80 FPS	440 FPS	120 FPS	86 FPS	180 FPS	3 FPS	110 FPS	475 FPS	305 FPS

these models on short segments and combine them into the final model. When the video is divided into M segments, VRAM and storage requirements scale M times accordingly. Moreover, since 4K4D and ENeRF require the source images as input, their reported storage cost also includes the video-encoded images. *Training time* reflects the convergence speed of each method. Similar to the *storage* cost, the training cost is summed over all segments for 3DGS, 4K4D, and 4DGS. *Rendering speed* is evaluated as the rendering FPS of each method when rendering to a real-time GUI.

5.2 Comparison Experiments

Both qualitative and quantitative comparisons are presented in Tab. 1 and Figs. 4 to 6. As shown in Tab. 1, our method achieves the best or comparable overall performance on all datasets across all evaluation metrics, including training cost, memory usage, speed, and image quality.

Compared to Gaussian-based methods like 3DGS and 4DGS, our model benefits from lower training costs, storage requirements, and faster inference speeds. While 3DGS [Kerbl et al. 2023] achieves good visual quality through per-frame training, its VRAM and storage usage scales unfavorably with the length of the video, making it unsuitable for handling long volumetric videos. Additionally, since 3DGS models each frame independently, it often produces videos with noticeable flickering artifacts. 4DGS [Yang et al. 2023b] extends 3DGS with a temporal axis to improve its capacity to model temporal dynamics but still suffers from high computation costs for training and storage.

Compared with the implicit method ENeRF [Lin et al. 2022], our model achieves an 80x speed improvement because ENeRF requires costly network evaluations for appearance modeling. As shown in Fig. 5, ENeRF tends to produce blurry results around occlusions and edges on the datasets with complex geometry like *MobileStage* [Xu et al. 2024b], degrading the visual quality a lot.

As for the hybrid method 4K4D [Xu et al. 2024b], it maintains a comparable inference speed to ours. However, the use of point clouds as geometry representation limits its ability to provide highly detailed appearances, especially on *Neural3DV* [Li et al. 2022], where point clouds are challenging to estimate accurately due to complex backgrounds. Moreover, like 3DGS, 4K4D employs a per-frame modeling approach, resulting in flickering artifacts.

Table 2. **Ablations on proposed components on the *Neural3DV* [Li et al. 2022] dataset.** Our Temporal Gaussian Hierarchy representation successfully reduces the GPU memory usage to a constant level and the Compact Appearance model significantly lowers our model size.

	PSNR ↑	LPIPS ↓	SSIM ↑	VRAM ↓	Storage ↓	Train. ↓	Render. ↑
w/o TGH	29.18	0.214	0.952	9.5 GB	0.093 GB	2.6 h	278 FPS
w/o App.	29.01	0.214	0.953	6.3 GB	0.238 GB	2.3 h	547 FPS
w/o Rend.	29.17	0.213	0.952	6.1 GB	0.092 GB	2.2 h	138 FPS
Ours	29.43	0.214	0.954	6.1 GB	0.92 GB	2.2 h	550 FPS

5.3 Results on Long Videos of *SelfCap*

The aforementioned experiments demonstrate the feasibility of our method for videos ranging from 40~50s. Compared to previous methods capable of handling only 1~2s, our approach achieves significant improvements. To further validate the potential for longer videos, we test our method on the new dataset *SelfCap*, which spans 6000 frames or even longer. Benefiting from our Temporal Gaussian Hierarchy, our method can maintain very low training costs, enabling it to represent extensive volumetric videos. In Fig. 7, we present visual results of videos from the *SelfCap* dataset. Our method showcases high-fidelity reconstruction results, particularly in complex areas with edges or occlusions, demonstrating superior rendering quality.

5.4 Ablation Study

We analyze our model components and components design choices on the *Neural3DV* [Li et al. 2022] dataset.

5.4.1 Ablations on Model Components.

The qualitative and quantitative results for ablations on model components are shown in Fig. 8 and Tab. 2.

Temporal Gaussian Hierarchy. We conduct experiments to evaluate the effectiveness of Temporal Gaussian Hierarchy. Without Temporal Gaussian Hierarchy (first row of Tab. 2), the model retrieves all 4D Gaussians to represent the training frames at each iteration. However, a significant portion of these Gaussians may not be relevant, resulting in high VRAM usage and slow iteration speed. Due to the substantial computational cost, the training is not

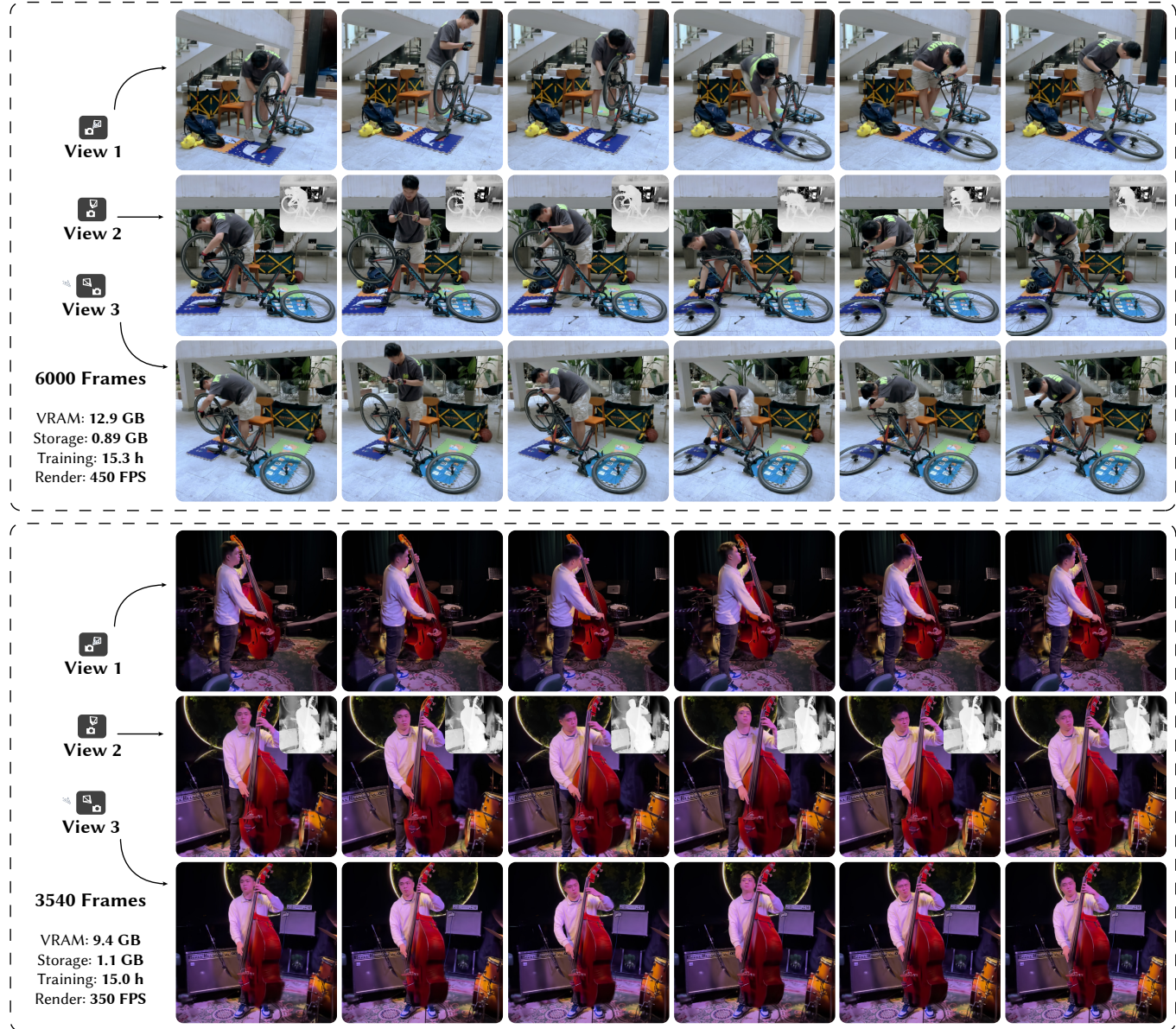


Fig. 7. **Qualitative results on long videos from our SelfCap.** We evaluate our method on very long videos consisting of 6000 and 3540 frames. Previous methods either suffer from high computational costs for training or low rendering quality, while our method addresses these challenges. The total number of 4D Gaussian points for these long sequences are 9.83M and 15.06M respectively.

performed sufficiently, resulting in degraded rendering results both quantitatively and qualitatively.

Compact Appearance Model. We investigate the effectiveness of Compact Appearance Model by comparing the results in the 2nd and 4th rows of Tab. 2. Our model occupies only 40% of the disk storage compared to the model with full spherical harmonics (SH) coefficients while maintaining the same rendering quality. This demonstrates the potential for our model to be extended to longer volumetric videos without incurring large storage overhead.

Real-time Rendering. We conducted an ablation study on the real-time rendering algorithm used in the inference stage. Compared to the vanilla rasterization pipeline of 3DGS (3rd row, Tab. 2), our algorithm achieves a 5x improvement in rendering speed, benefiting from the fast hardware rasterization.

5.4.2 Ablations on Temporal Gaussian Hierarchy.

We ablate the hyperparameters for Temporal Gaussian Hierarchy and analyze the effects of Temporal Gaussian Hierarchy as the frames of video increase.



Fig. 8. Qualitative comparison for ablations on proposed components.

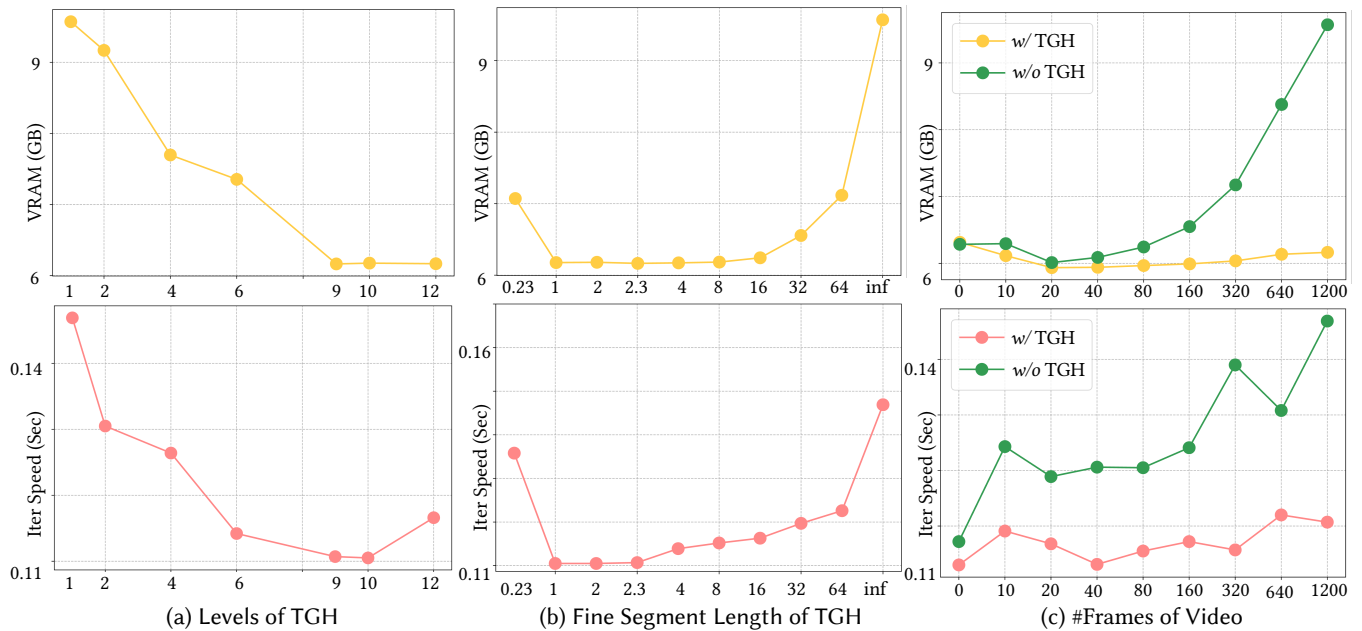


Fig. 9. **Ablations on Temporal Gaussian Hierarchy**: We analyze the effects of level L , root segment length S , and the number of frames in a training video on computational costs, including VRAM usage and iteration speed.

Number of Levels. We demonstrate quantitative comparisons of VRAM usage and iteration speed for our models trained with varying numbers of levels in Fig. 9 (a). It is important to note that our model with only 1 level will degrade into the conventional 4DGS with our Compact Appearance Model, resulting in increased VRAM usage and slower iteration speed during training. We observe that our model consistently achieves better efficiency as the number of levels increases. However, using a too-large level count introduces

overhead in the sampling and update process of Temporal Gaussian Hierarchy, resulting in lower iteration speed. Therefore, we use 9 levels as the default setting to train our model. Additionally, we include visual results for different levels of TGH. As shown in Fig. 10, the coarse level represents static scenes like the background, while the fine level with short temporal segments is used to model objects with dynamic motions.

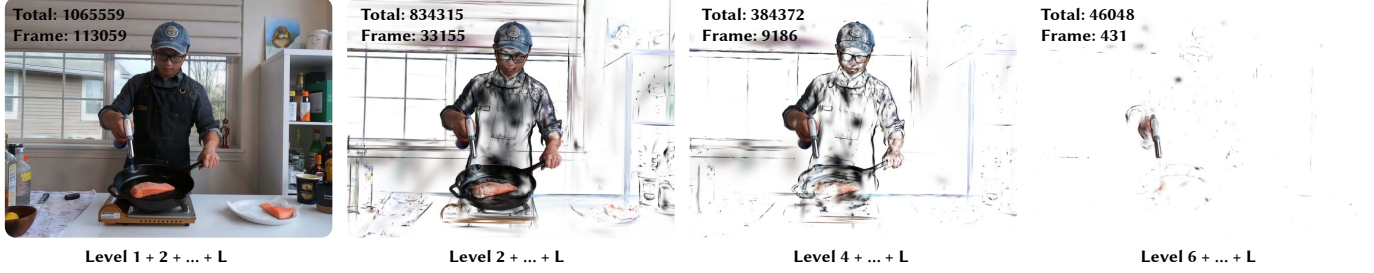


Fig. 10. Visual results for different levels of Temporal Gaussian Hierarchy on the 1200-frame Neural3DV [Li et al. 2022] dataset. The number of 4D Gaussians in each level range is shown on the top left corner. Note that the as the level increases, the movement speed of the Gaussians increase accordingly.

Table 3. Comparison on Storage and Image Quality with different gradient thresholds. Low threshold leads to all residual SH being enabled early, which might lead to slightly worse rendering quality, while large values might identify too small amount of view-dependent points.

	0	$1e^{-7}$	$1e^{-6}$ (Ours)	$1e^{-3}$	∞
Storage (MB)	238	94	92	65	65
PSNR \uparrow	29.01	28.93	29.44	29.06	28.96
SSIM \uparrow	0.953	0.953	0.954	0.951	0.950
LPIPS \downarrow	0.214	0.215	0.214	0.217	0.219

Root Segment Length. The root segment length is also a key factor affecting the computational efficiency of Temporal Gaussian Hierarchy. We conduct a comprehensive study with different lengths of the root segment. Fig. 9 (b) showcases that by increasing the segment length, the training cost initially decreases and then increases significantly. This is because when the segment length is either too long or too short, Gaussians influencing vastly different timestamps may be assigned to the same segment or placed into the global segment (Sec. 4), either due to the shortest segment being too long or the longest segment being too short. This increases the probability of sampling Gaussians that do not contribute to rendering at specific timestamps, resulting in an increase in both VRAM usage and iteration time. From our experiments, we found that a length of 10s is optimal, and we chose it as the default setting for our experiments.

Video Frames. As discussed in Sec. 3.2, one of the strengths of Temporal Gaussian Hierarchy is its nearly constant training cost regardless of the duration of video data. We evaluate the training cost of models with and without Temporal Gaussian Hierarchy as the number of training frames increases. As illustrated in Fig. 9 (c), our Temporal Gaussian Hierarchy structure maintains a constant VRAM cost and iteration speed even with very long video frames, whereas the model without Temporal Gaussian Hierarchy incurs significantly higher computational costs. This scalability facilitates the training of long volumetric videos using our methods.

5.4.3 Ablations on Appearance Model. We analyze the impact of the ratio parameter, λ_h , in the appearance model. We assess the disk storage of models with varying gradient ratios. Notably, when the ratio is 0, only the base color is utilized to model diffuse appearance, while a ratio of 1 indicates that we enable all SH coefficients to

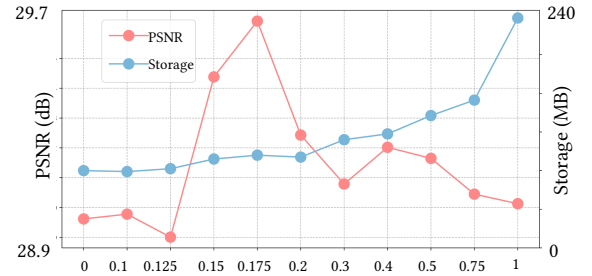


Fig. 11. Comparison on Storage cost and Image Quality with different ratio parameters. Storage cost decreases as the ratio drops. However, increasing the ratio does not necessarily lead to better results, as the model may overfit the scene. Based on these observations, we choose $\lambda_h=0.15$ for our method to balance storage efficiency and image quality.

model view-dependent effects. As illustrated in Fig. 11, we observe that the storage cost decreases as the ratio decreases. However, this reduction in storage comes at the expense of weakening the ability to model view-dependent effects, resulting in a decrease in image quality. Experimental results indicate that using a ratio of 0.15 can significantly reduce storage consumption without compromising rendering results. We also analyze the effect of different gradient thresholds when enabling residual SH, as shown in Tab. 3. According to the experiments, we select a gradient threshold of 0.000001 for our method.

We also compare the results of view-dependent effects for different models in Fig. 12. When the SH coefficients are zero, the rendering results only exhibit a diffuse appearance without any view-dependent effects. Our sparse SH representation retains the ability to express view-dependent effects similar to full SH while significantly reducing storage space, demonstrating the effectiveness of our Compact Appearance Model.

5.4.4 Ablations on the Hardware Rasterizer. In addition to comparing the rendering speed of the proposed hardware rasterizer [Shreiner et al. 2009] to the original software rasterizer [Kerbl et al. 2023] in Tab. 2, we also evaluate the impact of different sorting backends for the hardware rasterizer in Tab. 4. This ablation is done on a high-end consumer machine with an RTX 4090 GPU and an i9-13900K CPU. As shown in the table, using the CUDA backend [Paszke et al.

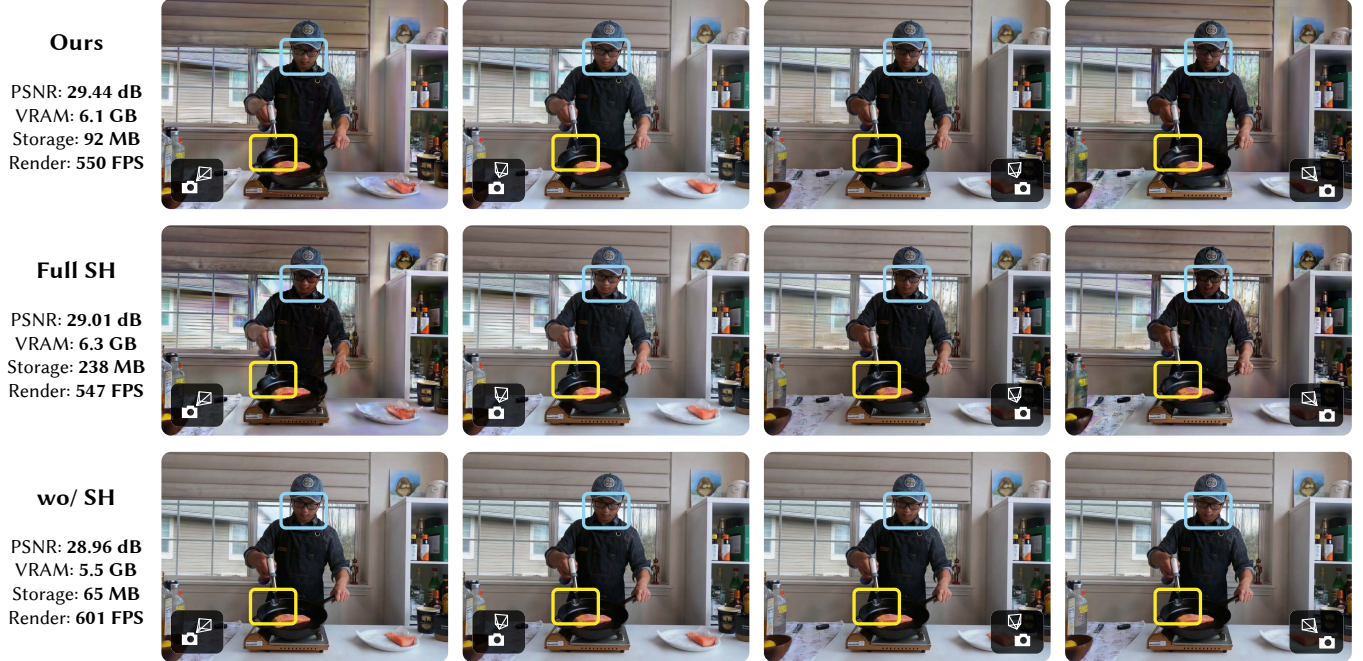


Fig. 12. **Qualitative comparisons for ablations on Compact Appearance Model.** We compare the view-dependent effects between our method and the model with full SH as well as without SH. Our proposed Compact Appearance Model successfully captures the view-dependency of the pan and face region.

Table 4. **Comparison on the sorting speed using different backends on an RTX 4090 and i9-13900K.** Sorting directly on the GPU using CUDA [Paszke et al. 2019] proves to be much more performant compared to the CPU-sorting [mkkellogg 2024] or Compute-Shader-sorting [Kopanas et al. 2024] implementation for the graphics-pipeline-based rasterizer.

Sorting Backend	CUDA (Ours)	CPU	Compute Shader
Million-Points / s \uparrow	8844	16.28	152.2

2019] greatly increases GPU utilization and sorting throughput and aids in our increased rendering speed compared to the CPU-sorting [mkkellogg 2024] or Compute-Shader-sorting backend [Kopanas et al. 2024] for the graphics-pipeline-based rasterizer.

5.4.5 Visualization on the Distribution of 4D Gaussians. In Fig. 13, Fig. 14 and Fig. 10 we visualize the distribution of 4D Gaussians in each level of the Temporal Gaussian Hierarchy across time and additionally show the rendering results of different levels. As shown by the figures, although the division of segments is uniform in the Temporal Gaussian Hierarchy, the number of 4D Gaussians in each segment is different, achieving a non-uniform subdivision of representational power across time.

6 CONCLUSION

We proposed temporal Gaussian hierarchy, a novel 4D scene representation to reconstruct long volumetric videos with low storage cost from multi-view RGB videos. The representation is built based on the observation that dynamic scenes typically exhibit varying

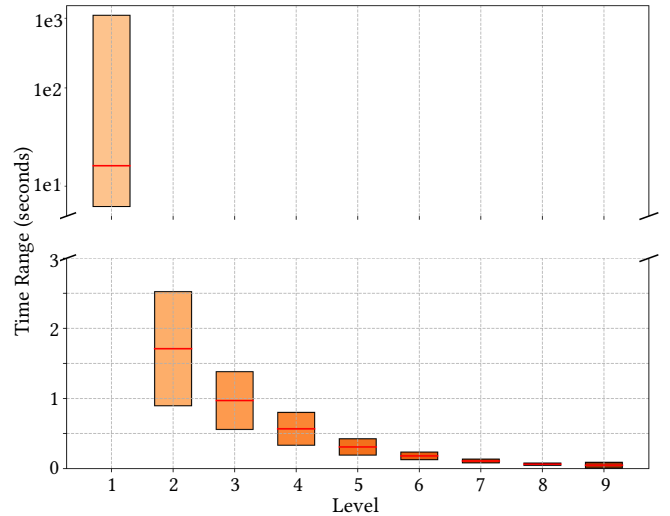


Fig. 13. **Visualization on the mean and standard deviation of the range of the 4D Gaussians on the 1200-frame (40s) flame_salmon sequence of the Neural3DV dataset determined by Eq. (4).**

degrees of temporal redundancy, as there are generally scene areas with different motions. Specifically, the Gaussian hierarchy consists of multiple levels, and each level independently describes regions of the scene with different degrees of content change based on a set of segments. Our approach stores a set of Gaussian primitives

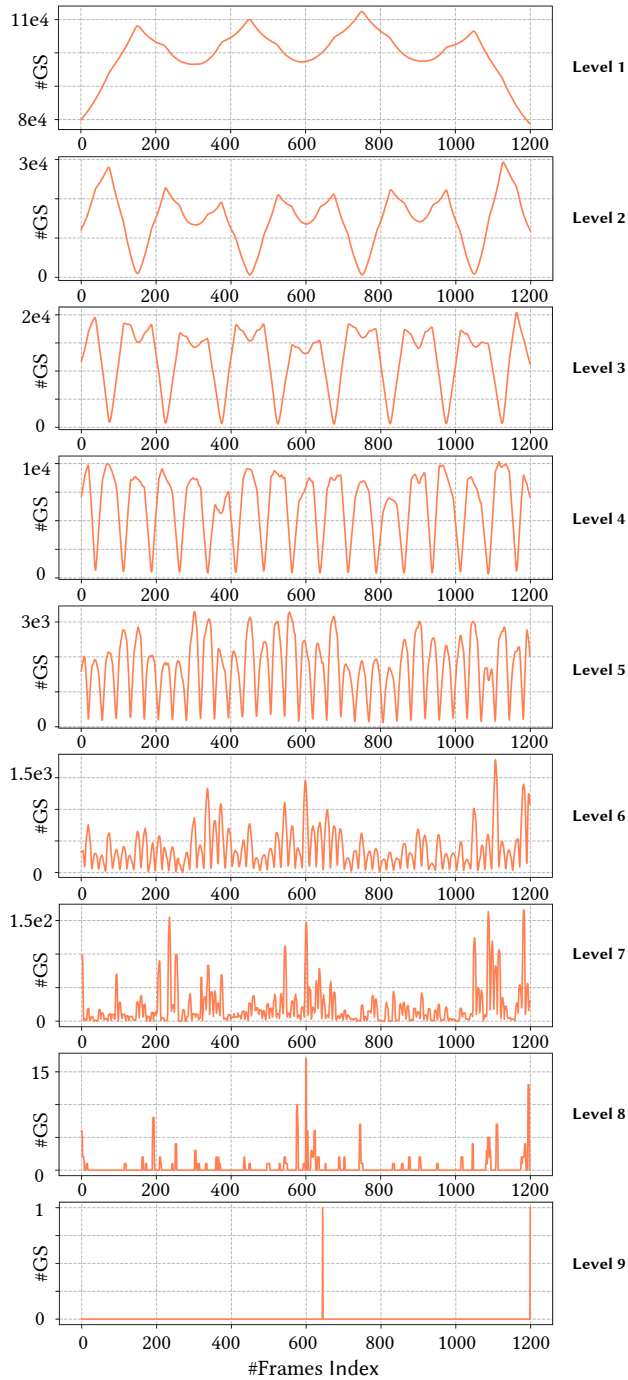


Fig. 14. Visualization on the number of 4D Gaussians for each of the 9 levels across the 1200-frame (40s) duration of the *flame_salmon* sequence of the *Neural3DV* dataset.

in these segments and adaptively shares them to depict the scene content across various temporal scales. We further exploited the tree-like structure of the hierarchy to efficiently represent the scene at a time step using a subset of Gaussian primitives, resulting in nearly constant GPU memory usage during the training or rendering process, irrespective of the volumetric video’s length. In addition, we designed a Compact Appearance Model that integrated diffuse and view-dependent Gaussians to reduce the model size. We also developed a rasterization pipeline for Gaussian primitives leveraging hardware-accelerated techniques to enhance rendering efficiency. In conclusion, both qualitative and quantitative evaluations confirm that our method surpasses existing baselines, offering state-of-the-art visual quality and rendering speed. Moreover, our method requires significantly less training cost and memory usage, facilitating the reconstruction and rendering of long volumetric videos.

7 DISCUSSION

Limitation. Although our work shows significant improvement on long volumetric videos, it still has some limitations. First, our reconstruction system is not real-time, requiring several hours to transform volumetric videos into our 4D representation. To further improve training efficiency, we could instill a stronger geometry prior or regularize the distribution of Gaussian primitives. Moreover, our method requires semi-dense views to adequately cover dynamic scenes, and it doesn’t generalize well in a sparse-view setting. Inspired by prior works [Wu et al. 2023a], we plan to use the strong generative priors in diffusion models [Rombach et al. 2022] to improve sparse-view reconstruction results.

ACKNOWLEDGMENTS

The authors would like to acknowledge support from NSFC (No. 62172364), Information Technology Center, and State Key Lab of CAD&CG, Zhejiang University.

REFERENCES

- Naveed Ahmed, Christian Theobalt, Christian Rossl, Sebastian Thrun, and Hans-Peter Seidel. 2008. Dense correspondence finding for parametrization-free animation reconstruction from video.
- Kara-Ali Aliev, Artem Sevastopolsky, Maria Kolos, Dmitry Ulyanov, and Victor Lempitsky. 2020. Neural point-based graphics. In *ECCV*.
- Aljaz Bozic, Michael Zollhofer, Christian Theobalt, and Matthias Nießner. 2020. Deep-deform: Learning non-rigid rgb-d reconstruction with semi-supervised data. In *CVPR*.
- Ang Cao and Justin Johnson. 2023. HexPlane: A Fast Representation for Dynamic Scenes. (2023).
- Joel Carranza, Christian Theobalt, Marcus A Magnor, and Hans-Peter Seidel. 2003. Free-viewpoint video of human actors. *ACM transactions on graphics (TOG)* 22, 3 (2003), 569–577.
- Anpei Chen, Zexiang Xu, Andreas Geiger, Jingyi Yu, and Hao Su. 2022. Tensor4: Tensorial radiance fields. In *European Conference on Computer Vision*. Springer.
- Anpei Chen, Zexiang Xu, Fuqiang Zhao, Xiaoshuai Zhang, Fanbo Xiang, Jingyi Yu, and Hao Su. 2021. Mvsnerf: Fast generalizable radiance field reconstruction from multi-view stereo. In *ICCV*.
- Zhiqin Chen, Thomas Funkhouser, Peter Hedman, and Andrea Tagliasacchi. 2023. Mobilenerf: Exploiting the polygon rasterization pipeline for efficient neural field rendering on mobile architectures. In *CVPR*.
- Alvaro Collet, Ming Chuang, Pat Sweeney, Don Gillett, Dennis Evseev, David Calabrese, Hugues Hoppe, Adam Kirk, and Steve Sullivan. 2015. High-quality streamable free-viewpoint video. *ACM Transactions on Graphics (ToG)* 34, 4 (2015), 1–13.
- Yilun Du, Yanan Zhang, Hong-Xing Yu, Joshua B Tenenbaum, and Jiajun Wu. 2021. Neural radiance flow for 4d view synthesis and video processing. In 2021 IEEE. In *CVF International Conference on Computer Vision (ICCV)*. 14304–14314.

- Yuanxing Duan, Fangyin Wei, Qiyu Dai, Yuhang He, Wenzheng Chen, and Baoquan Chen. 2024. 4D Gaussian Splatting: Towards Efficient Novel View Synthesis for Dynamic Scenes. *arXiv preprint arXiv:2402.03307* (2024).
- Jiemin Fang, Taoran Yi, Xinggang Wang, Lingxi Xie, Xiaopeng Zhang, Wenyu Liu, Matthias Nießner, and Qi Tian. 2022. Fast dynamic radiance fields with time-aware neural voxels. In *SIGGRAPH Asia 2022 Conference Papers*.
- Sara Fridovich-Keil, Giacomo Meanti, Frederik Rahbæk Warburg, Benjamin Recht, and Angjoo Kanazawa. 2023. K-Planes: Explicit Radiance Fields in Space, Time, and Appearance. In *CVPR*.
- Sara Fridovich-Keil, Alex Yu, Matthew Tancik, Qinhong Chen, Benjamin Recht, and Angjoo Kanazawa. 2022. Plenoxels: Radiance fields without neural networks. In *CVPR*.
- Stephan J Garbin, Marek Kowalski, Matthew Johnson, Jamie Shotton, and Julien Valentin. 2021. Fastnerf: High-fidelity neural rendering at 200fps.
- Jon Hasselgren, Nikolai Hofmann, and Jacob Munkberg. 2022. Shape, light, and material decomposition from images using monte carlo rendering and denoising. *NeurIPS* (2022).
- Peter Hedman, Pratul P Srinivasan, Ben Mildenhall, Jonathan T Barron, and Paul Debevec. 2021. Baking neural radiance fields for real-time view synthesis.
- David A Huffman. 1952. A method for the construction of minimum-redundancy codes. *Proceedings of the IRE* 40, 9 (1952), 1098–1101.
- Hanbyul Joo, Hao Liu, Lei Tan, Lin Gui, Bart Nabbe, Iain Matthews, Takeo Kanade, Shohei Nobuhara, and Yaser Sheikh. 2015. Panoptic studio: A massively multiview system for social motion capture. In *Proceedings of the IEEE international conference on computer vision*. 3334–3342.
- HyunJun Jung, Nikolas Brasch, Jifei Song, Eduardo Perez-Pellitero, Yiren Zhou, Zhihao Li, Nassir Navab, and Benjamin Busam. 2023. Deformable 3d gaussian splatting for animatable human avatars. *arXiv preprint arXiv:2312.15059* (2023).
- Bernhard Kerbl, Georgios Kopanas, Thomas Leimkühler, and George Drettakis. 2023. 3D gaussian splatting for real-time radiance field rendering. *ACM Transactions on Graphics (TOG)* 42, 4 (2023), 1–14.
- Diederik P Kingma and Jimmy Ba. 2014. Adam: A method for stochastic optimization. *arXiv preprint arXiv:1412.6980* (2014).
- Georgios Kopanas, Bernhard Kerbl, Antoine Guédon, and Jonathon Luiten. 2024. 3D Gaussian Splatting Tutorial. <https://3dgsutorial.github.io/> International Conference on 3D Vision Tutorial.
- Alex Krizhevsky, Ilya Sutskever, and Geoffrey E Hinton. 2012. Imagenet classification with deep convolutional neural networks. *Advances in neural information processing systems* 25 (2012).
- Jonas Kulhanek and Torsten Sattler. 2023. Tetra-nerf: Representing neural radiance fields using tetrahedra. In *ICCV*.
- Christoph Lassner and Michael Zollhofer. 2021. Pulsar: Efficient sphere-based neural rendering. In *CVPR*.
- Tianye Li, Mira Slavcheva, Michael Zollhoefer, Simon Green, Christoph Lassner, Changil Kim, Tanner Schmidt, Steven Lovegrove, Michael Goesele, Richard Newcombe, et al. 2022. Neural 3d video synthesis from multi-view video. In *Proceedings of the IEEE/CVF Conference on Computer Vision and Pattern Recognition*. 5521–5531.
- Zhengqi Li, Qianqian Wang, Forrester Cole, Richard Tucker, and Noah Snavely. 2023. Dynibar: Neural dynamic image-based rendering. In *Proceedings of the IEEE/CVF Conference on Computer Vision and Pattern Recognition*. 4273–4284.
- Haotong Lin, Sida Peng, Zhen Xu, Tao Xie, Xingyi He, Hujun Bao, and Xiaowei Zhou. 2023b. High-Fidelity and Real-Time Novel View Synthesis for Dynamic Scenes. In *SIGGRAPH Asia Conference Proceedings*.
- Haotong Lin, Sida Peng, Zhen Xu, Yunzhi Yan, Qing Shuai, Hujun Bao, and Xiaowei Zhou. 2022. Efficient Neural Radiance Fields for Interactive Free-viewpoint Video. In *SIGGRAPH Asia Conference Proceedings*.
- Youtian Lin, Zuozhuo Dai, Siyu Zhu, and Yao Yao. 2023a. Gaussian-flow: 4d reconstruction with dynamic 3d gaussian particle. *arXiv preprint arXiv:2312.03431* (2023).
- Huan Ling, Seung Wook Kim, Antonio Torralba, Sanja Fidler, and Karsten Kreis. 2023. Align your gaussians: Text-to-4d with dynamic 3d gaussians and composed diffusion models. *arXiv preprint arXiv:2312.13763* (2023).
- Stephen Lombardi, Tomas Simon, Jason Saragih, Gabriel Schwartz, Andreas Lehrmann, and Yaser Sheikh. 2019. Neural volumes: Learning dynamic renderable volumes from images. *arXiv preprint arXiv:1906.07751* (2019).
- Xiaoxiao Long, Cheng Lin, Peng Wang, Taku Komura, and Wenping Wang. 2022. Sparseneus: Fast generalizable neural surface reconstruction from sparse views.
- Fan Lu, Yan Xu, Guang Chen, Hongsheng Li, Kwan-Yee Lin, and Changjun Jiang. 2023. Urban radiance field representation with deformable neural mesh primitives. In *ICCV*.
- Zhicheng Lu, Xiang Guo, Le Hui, Tianrui Chen, Min Yang, Xiao Tang, Feng Zhu, and Yuchao Dai. 2024. 3d geometry-aware deformable gaussian splatting for dynamic view synthesis. *arXiv preprint arXiv:2404.06270* (2024).
- Jonathon Luiten, Georgios Kopanas, Bastian Leibe, and Deva Ramanan. 2024. Dynamic 3D Gaussians: Tracking by Persistent Dynamic View Synthesis. In *3DV*.
- Lars Mescheder, Michael Oechsle, Michael Niemeyer, Sebastian Nowozin, and Andreas Geiger. 2019. Occupancy Networks: Learning 3D Reconstruction in Function Space. In *CVPR*.
- Ben Mildenhall, Pratul P Srinivasan, Matthew Tancik, Jonathan T Barron, Ravi Ramamoorthi, and Ren Ng. 2021. Nerf: Representing scenes as neural radiance fields for view synthesis. *Commun. ACM* 65, 1 (2021), 99–106.
- mikkellogg. 2024. GaussianSplats3D. <https://github.com/mikkellogg/GaussianSplats3D>.
- Claus Müller. 2006. *Spherical harmonics*. Vol. 17. Springer.
- Thomas Müller, Alex Evans, Christoph Schied, and Alexander Keller. 2022. Instant neural graphics primitives with a multiresolution hash encoding. *ACM transactions on graphics (TOG)* (2022).
- Richard A Newcombe, Dieter Fox, and Steven M Seitz. 2015. Dynamicfusion: Reconstruction and tracking of non-rigid scenes in real-time.
- Jeong Joon Park, Peter Florence, Julian Straub, Richard Newcombe, and Steven Lovegrove. 2019. Deepsdf: Learning continuous signed distance functions for shape representation. In *Proceedings of the IEEE/CVF conference on computer vision and pattern recognition*. 165–174.
- Keunhong Park, Utkarsh Sinha, Jonathan T Barron, Sofien Bouaziz, Dan B Goldman, Steven M Seitz, and Ricardo Martin-Brualla. 2021a. Nerfies: Deformable neural radiance fields. In *Proceedings of the IEEE/CVF International Conference on Computer Vision*. 5865–5874.
- Keunhong Park, Utkarsh Sinha, Peter Hedman, Jonathan T Barron, Sofien Bouaziz, Dan B Goldman, Ricardo Martin-Brualla, and Steven M Seitz. 2021b. Hypernerf: A higher-dimensional representation for topologically varying neural radiance fields. *arXiv preprint arXiv:2106.13228* (2021).
- Adam Paszke, Sam Gross, Francisco Massa, Adam Lerer, James Bradbury, Gregory Chanan, Trevor Killeen, Zeming Lin, Natalia Gimelshein, Luca Antiga, Alban Desmaison, Andreas Kopf, Edward Yang, Zachary DeVito, Martin Raison, Alykhan Tejani, Sasank Chilamkurthy, Benoit Steiner, Lu Fang, Junjie Bai, and Soumith Chintala. 2019. PyTorch: An Imperative Style, High-Performance Deep Learning Library. In *NeurIPS*.
- Albert Pumarola, Enric Corona, Gerard Pons-Moll, and Francesc Moreno-Noguer. 2021a. D-nerf: Neural radiance fields for dynamic scenes. In *Proceedings of the IEEE/CVF Conference on Computer Vision and Pattern Recognition*. 10318–10327.
- Albert Pumarola, Enric Corona, Gerard Pons-Moll, and Francesc Moreno-Noguer. 2021b. D-nerf: Neural radiance fields for dynamic scenes.
- Ruslan Rakhimov, Andrei-Timotei Ardelean, Victor Lempitsky, and Evgeny Burnaev. 2022. Npbg++: Accelerating neural point-based graphics. In *CVPR*.
- Jiawei Ren, Liang Pan, Jiaxiang Tang, Chi Zhang, Ang Cao, Gang Zeng, and Ziwei Liu. 2023. Dreamgaussian4d: Generative 4d gaussian splatting. *arXiv preprint arXiv:2312.17142* (2023).
- Robin Rombach, Andreas Blattmann, Dominik Lorenz, Patrick Esser, and Björn Ommer. 2022. High-Resolution Image Synthesis With Latent Diffusion Models. In *Proceedings of the IEEE/CVF Conference on Computer Vision and Pattern Recognition (CVPR)*.
- Darius Rückert, Linus Franke, and Marc Stamminger. 2022. Adop: Approximate differentiable one-pixel point rendering. *ACM Transactions on Graphics (ToG)* (2022).
- Jason Sanders and Edward Kandrot. 2010. *CUDA by example: an introduction to general-purpose GPU programming*. Addison-Wesley Professional.
- Johannes L Schonberger and Jan-Michael Frahm. 2016. Structure-from-motion revisited. In *Proceedings of the IEEE conference on computer vision and pattern recognition*. 4104–4113.
- Dave Shreiner et al. 2009. *OpenGL programming guide: the official guide to learning OpenGL, versions 3.0 and 3.1*. Pearson Education.
- Towaki Takikawa, Alex Evans, Jonathan Tremblay, Thomas Müller, Morgan McGuire, Alec Jacobson, and Sanja Fidler. 2022. Variable bitrate neural fields. In *ACM SIGGRAPH 2022 Conference Proceedings*.
- Jiaxiang Tang, Xiaokang Chen, Jingbo Wang, and Gang Zeng. 2022. Compressible-composable nerf via rank-residual decomposition. *NeurIPS* (2022).
- Edgar Tretschk, Ayush Tewari, Vladislav Golyanik, Michael Zollhofer, Christoph Lassner, and Christian Theobalt. 2021a. Non-rigid neural radiance fields: Reconstruction and novel view synthesis of a dynamic scene from monocular video.
- Edgar Tretschk, Ayush Tewari, Vladislav Golyanik, Michael Zollhofer, Christoph Lassner, and Christian Theobalt. 2021b. Non-Rigid Neural Radiance Fields: Reconstruction and Novel View Synthesis of a Dynamic Scene From Monocular Video. In *IEEE International Conference on Computer Vision (ICCV)*. IEEE.
- Liao Wang, Jiakai Zhang, Xinhang Liu, Fuqiang Zhao, Yanshun Zhang, Yingliang Zhang, Minye Wu, Jingyi Yu, and Lan Xu. 2022. Fourier PlenOctrees for Dynamic Radiance Field Rendering in Real-Time. In *Proceedings of the IEEE/CVF Conference on Computer Vision and Pattern Recognition (CVPR)*. 13524–13534.
- Qianqian Wang, Zhicheng Wang, Kyle Genova, Pratul P Srinivasan, Howard Zhou, Jonathan T Barron, Ricardo Martin-Brualla, Noah Snavely, and Thomas Funkhouser. 2021. Ibrnet: Learning multi-view image-based rendering.
- Zhou Wang, Alan C Bovik, Hamid R Sheikh, and Eero P Simoncelli. 2004a. Image quality assessment: from error visibility to structural similarity. *IEEE transactions on image processing* 13, 4 (2004), 600–612.
- Zhou Wang, Alan C Bovik, Hamid R Sheikh, and Eero P Simoncelli. 2004b. Image quality assessment: from error visibility to structural similarity. *IEEE transactions on image processing* (2004).

- Guanjun Wu, Taoran Yi, Jiemin Fang, Lingxi Xie, Xiaopeng Zhang, Wei Wei, Wenyu Liu, Qi Tian, and Wang Xinggang. 2023b. 4D Gaussian Splatting for Real-Time Dynamic Scene Rendering. *arXiv preprint arXiv:2310.08528* (2023).
- Minye Wu, Yuehao Wang, Qiang Hu, and Jingyi Yu. 2020. Multi-view neural human rendering. In *Proceedings of the IEEE/CVF Conference on Computer Vision and Pattern Recognition*. 1682–1691.
- Rundi Wu, Ben Mildenhall, Philipp Henzler, Keunhong Park, Ruiqi Gao, Daniel Watson, Pratul P Srinivasan, Dor Verbin, Jonathan T Barron, Ben Poole, et al. 2023a. Reconfusion: 3d reconstruction with diffusion priors. *arXiv preprint arXiv:2312.02981* (2023).
- Zhen Xu, Sida Peng, Chen Geng, Linzhan Mou, Zihan Yan, Jiaming Sun, Hujun Bao, and Xiaowei Zhou. 2024a. Relightable and Animatable Neural Avatar from Sparse-View Video. In *CVPR*.
- Zhen Xu, Sida Peng, Haotong Lin, Guangzhao He, Jiaming Sun, Yujun Shen, Hujun Bao, and Xiaowei Zhou. 2024b. 4K4D: Real-Time 4D View Synthesis at 4K Resolution. In *CVPR*.
- Zhen Xu, Tao Xie, Sida Peng, Haotong Lin, Qing Shuai, Zhiyuan Yu, Guangzhao He, Jiaming Sun, Hujun Bao, and Xiaowei Zhou. 2023. EasyVolcap: Accelerating Neural Volumetric Video Research. (2023).
- Ziyi Yang, Xinyu Gao, Wen Zhou, Shaohui Jiao, Yuqing Zhang, and Xiaogang Jin. 2023a. Deformable 3D Gaussians for High-Fidelity Monocular Dynamic Scene Reconstruction. *arXiv preprint arXiv:2309.13101* (2023).
- Zeyu Yang, Hongye Yang, Zijie Pan, Xiatian Zhu, and Li Zhang. 2023b. Real-time Photorealistic Dynamic Scene Representation and Rendering with 4D Gaussian Splatting. *arXiv preprint arXiv:2310.10642* (2023).
- Alex Yu, Vickie Ye, Matthew Tancik, and Angjoo Kanazawa. 2021. pixelnerf: Neural radiance fields from one or few images.
- Tao Yu, Kaiwen Guo, Feng Xu, Yuan Dong, Zhaoqi Su, Jianhui Zhao, Jianguo Li, Qionghai Dai, and Yebin Liu. 2017. Bodyfusion: Real-time capture of human motion and surface geometry using a single depth camera.
- Tao Yu, Zerong Zheng, Kaiwen Guo, Jianhui Zhao, Qionghai Dai, Hao Li, Gerard Pons-Moll, and Yebin Liu. 2018. Doublefusion: Real-time capture of human performances with inner body shapes from a single depth sensor.
- Richard Zhang, Phillip Isola, Alexei A Efros, Eli Shechtman, and Oliver Wang. 2018a. The unreasonable effectiveness of deep features as a perceptual metric. In *Proceedings of the IEEE conference on computer vision and pattern recognition*. 586–595.
- Richard Zhang, Phillip Isola, Alexei A Efros, Eli Shechtman, and Oliver Wang. 2018b. The Unreasonable Effectiveness of Deep Features as a Perceptual Metric. In *CVPR*.